University of Bath

A realistic simulation framework to evaluate ionospheric tomography

Jon Bruno [*], Cathryn N. Mitchell, Karl H.A. Bolmgren, Ben A. Witvliet

Centre for Space, Atmospheric and Oceanic Science, Department of Electronic and Electrical Engineering, University of Bath, UK

Abstract

Observation of the 3-dimensional (3-D) electron density of the ionosphere is useful to study large-scale physical processes in space weather events. Ionospheric data assimilation and ionospheric tomography are methods that can create an image of the 3-D electron density distribution. While multiple techniques have been developed over the past 30 years, there are relatively few studies that show the accuracy of the algorithms. This paper outlines a novel simulation approach to test the quality of an ionospheric tomographic inversion. The approach uses observations from incoherent scatter radar (ISR) scans and extrapolates them spatially to create a realistic ionospheric representation. A set of total electron content (TEC) measurements can then be simulated using real geometries from satellites and ground receivers. This data set, for which the 'truth' ionosphere is known, is used as input for a tomographic inversion algorithm to estimate the spatial distribution of electron density. The reconstructed ionospheric maps are compared with the truth ionosphere to calculate the difference between the images and the truth.

To demonstrate the effectiveness of this simulation framework, an inversion algorithm called MIDAS (Multi-Instrument Data Analysis Software) is evaluated for three geographic regions with differing receiver networks. The results show the importance of the distribution and density of GPS receivers and the use of a realistic prior conditioning of the vertical electron density profile. This paper demonstrates that when these requirements are met, MIDAS can reliably estimate the ionospheric electron density. When the region under study is well covered by GPS receivers, as in mainland Europe or North America, the errors in vertical total electron content (vTEC) are smaller than 1 TECu (2–4%) . In regions with fewer and more sparsely distributed receivers, the errors can be as high as 20–40%. This is caused by poor data coverage and poor spatial resolution of the reconstruction, which has an important effect on the calibration process of the algorithm.

1. Introduction

The ionosphere, the ionised region of the Earth's atmosphere at altitudes between approximately 80 and 1000 km, is mainly created by the interaction between the Sun's electromagnetic emissions and the Earth's atmosphere. It changes both spatially and temporally and is influenced by changes in solar emissions, atmospheric dynamics and interplanetary and geomagnetic fields (Hargreaves, 1992).

Free electrons within the ionosphere cause electromagnetic wave refraction and delay, and these effects depend on the local electron density and the frequency of the wave (McNamara, 1991; Leitinger, 1999). This property makes dual-frequency Global Navigation Satellite System (GNSS) signals ideal for ionospheric sensing. By recording the phase and time delay of the two signals at the two frequencies, the frequency-dependent aspect can be eliminated and the Total Electron Content (TEC) along the satellite-receiver ray path can be derived (Mannucci et al., 1998). It must be noted that TEC measurements are susceptible to different error sources, such as satellite and receiver

* Corresponding author.
E-mail address: j.bruno@bath.ac.uk (J. Bruno).

biases (Wilson and Mannucci, 1993), so the use of them in tomographic imaging requires knowledge of these biases and calibration.

To determine the distribution and density of free electrons in the ionosphere, radio tomographic techniques were first proposed by Austen et al. (1986), which were further improved to obtain 3-D and 4-D specification of the ionosphere (Fremouw et al., 1992; Hernandez-Pajares et al., 1998; Bust et al., 2007). Ionospheric tomography has had an important impact on different fields, especially on GNSS positioning and timing corrections (Rose et al., 2014; Allain and Mitchell, 2008; Hernández-Pajares et al., 2000). However, assessing the accuracy of these algorithms is challenging because a specification of the true ionosphere is not available as reference. Therefore, in this paper, a simulation framework is developed and used to assess the accuracy of the tomographic inversion algorithm called MIDAS (Multi-Instrument Data Analysis Software) (Mitchell and Spencer, 2003). The method may also be adapted for other algorithms.

Tomography is the reconstruction of two, three or four-dimensional images from line-integral measurements influenced by the imaged object (Radon, 1917). In the case of ionospheric tomography, the line-integral observation is the TEC:

$$TEC = \int_{S}^{R} N(s)ds \tag{1}$$

in which N is the electron density per unit volume and s the distance along the ray path from satellite (S) to receiver (R). TEC is the columnar electron density and is expressed in TEC Units (TECu), where 1 $TECu = 10^{16}$ electrons/m^2. When a GNSS receiver network consisting of sufficient number of receivers with large spatial coverage is available, TEC measurements can be used for ionospheric tomography (Bust and Mitchell, 2008). Individual TEC measurements provide no information about the electron distribution along the ray path, but a series of them crossing each other in the ionosphere can be inverted into spatial maps of electron density.

In ionospheric tomography, the electron density may be assumed constant within a sufficiently small volume around a point (a 'voxel') in the ionosphere. The contribution to the measured TEC of each intersection of the ray with a voxel is therefore the multiplication of that electron density and the length of the intersection. The TEC of a single ray path is the summation of these segments. For n ray paths and m voxels, this may be expressed as:

$$\vec{b} = \sum_{i=1}^{i=n}\sum_{j=1}^{j=m} A_{i,j} \times x_j \tag{2}$$

where $\vec{b}$ contains all the TEC measurements, $A_{i,j}$ is an array that contains the lengths of the intersections of the n ray paths with each of the m voxels, and $\vec{x}$ is a vector containing the electron density in each of the m voxels.
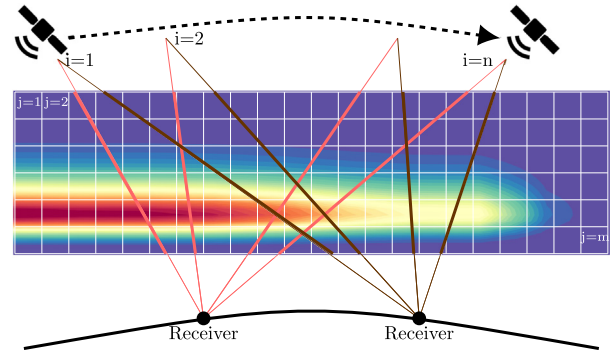

Fig. 1. Ionospheric tomography example, showing ray paths intersecting a grid of voxels.

Fig. 1 shows a graphical example of voxels and rays in a two-dimensional representation of the ionosphere.

The same equation can be expressed in matrix form as:

$$\mathbf{A}\vec{x} = \vec{b} \tag{3}$$

where $\mathbf{A}$ is an $n \times m$ matrix of the path lengths within each voxel, $\vec{x}$ is the electron density within each of the m voxels, and $\vec{b}$ are the n observed TECs.

It is important to remark that, particularly when only ground-based receivers are used, ionospheric tomography is limited by the satellite-to-receiver geometry. This leads to a lack of horizontal ray-paths through the ionosphere. Not having enough data to cover the entire geographical area with evenly-spread receivers is another limitation. Mathematically these limitations may cause the inversion to be underdetermined. To overcome this difficulty, a mapping matrix $\mathbf{M}$ is used to transform the problem to one for which the unknowns are coefficients of orthonormal basis functions, the combination of which will produce the final image of electron density (Mitchell and Spencer, 2003; Fremouw et al., 1992). The problem is now expressed mathematically as:

$$\mathbf{A}\mathbf{M}\vec{W} = \vec{b} \tag{4}$$

where the matrix $\mathbf{M}$ defines the mapping from a voxel-based representation to an orthonormal representation by using basis functions, such that $\mathbf{A}\mathbf{M}$ defines a basis set of line integrations of electron density through the geometry volume defined by $\mathbf{A}$. Once $\vec{W}$ is calculated by solving the inverse problem, the electron density is given by:

$$\vec{x} = \mathbf{M}\vec{W} \tag{5}$$

The method can be used to provide full three (or even four if time is considered) dimensional images of the ionosphere, which is more accurate than thin shell ionospheric mapping (Hernández-Pajares et al., 1999; Allain and Mitchell, 2010). The software that is analysed in this paper, MIDAS, uses a variation of this technique for the reconstruction, where the horizontal electron density gradient is given by discrete functions.

Ionospheric tomography has previously been verified in individual studies using different experimental data sources, such as incoherent scatter radars (Pryse and Kersley, 1992; Walker et al., 1996; Mitchell et al., 1995; Meggs et al., 2005) or ionosondes (Hernandez-Pajares et al., 1998; Lee et al., 2008). Such a verification is complicated by the fact that all instruments have associated measurement errors. Therefore, the evaluation is limited by the accuracy of the instruments. Furthermore, these systems do not cover large regions of the Earth. In this paper this issue is overcome by creating a simulation framework that is based upon incoherent scatter radar (ISR) observations and their extrapolation over a wide area, thus benefiting from the realism of the ISR scans while eliminating the effect of instrument precision.

ISRs were first introduced by Gordon (1958). Essentially, ISR involves back scatter from plasma waves that are generated in the ionosphere (Beynon and Williams, 1978). The key feature of this instrument is that it is able to observe above the peak electron density regions in the ionosphere.

In addition to their contribution to the physical understanding of the ionosphere, an important application of ISR has been to provide independent verification for other experimental techniques, such as ionospheric tomography (Meggs et al., 2005). It provides accurate and independent ionospheric observations of electron density, which helps to validate the performance of tomographic inversion algorithms (Walker et al., 1996; Bust et al., 2007). The European Incoherent Scatter (EISCAT) (Rishbeth and Williams, 1985) was used for the independent verification of ionospheric tomography for the first time in 1992, as reported by Pryse and Kersley (1992).

In this paper, ISR scans are used to produce computer representations of the ionosphere that are then used to test an ionospheric imaging algorithm, with the aim of evaluating the accuracy and finding the best approach for imaging the ionosphere. Data from two different ISRs are used in this paper. The first one, the EISCAT radar, has two radar systems (a VHF and a UHF transmitter, both co-located with their receivers) near Tromsø, Norway (19.2° E longitude and 69.6° N latitude). The second ISR is located at the Millstone Hill observatory (71.5° W longitude and 42.6° N latitude) in Massachusetts, USA. Two-dimensional (electron density vs. latitude and height) scans of the ionosphere were selected.

It is helpful at this stage to define some of the terminology to be used in this paper. 'Ionospheric model' refers to a 3-D computer representation of the ionospheric electron density. 'Simulation' refers to the use of these simulated observations as input to a tomographic algorithm to create an image of the ionospheric model. 'Reconstruction' refers to the use of these simulated observations to create a representation of the ionospheric model. The analogous terms in a real experimental situation would be ionospheric electron density (ionospheric model), observations (simulated observations) and reconstruction/inversion/image (reconstruction).

The paper is structured as follows. In Section 2, the creation of the ionospheric models and the simulated observations are introduced. Then, in Section 3, the important parameters needed for the reconstruction are described and selected. Finally, the results are shown and discussed in Section 4.

2. Definition of the 'truth' ionospheric models and simulated observations

To test the accuracy of the ionospheric tomography algorithms, a truth ionosphere is needed, with an associated data set of GNSS TEC-measurements. These TEC-measurements can be inverted using a tomographic algorithm, after which the reconstructions can be compared with the truth to assess accuracy.

2.1. Specification of the 'truth' ionosphere

Two truth computer ionospheric models were created using observations from two different ISRs. The two-dimensional scan (Meggs et al., 2005) used to create the first ionospheric input model from the EISCAT at Tromsø, images the ionosphere from latitude 64° to 78° N at longitude 19° E, reaching 600 km of altitude above the Earth's surface. The scan was obtained on 2002-01-07 at 12:30 UT, and is shown in Fig. 2a. The second model was created using a scan from the Millstone Hill ISR at 16:15 UT on 2010-07-30, as seen in Fig. 2b. This scan measured the electron density of the ionosphere from latitude 42° to 48° N at longitude 72° W and up to 600 km height.

As the ISR measurements are performed in a 2-D plane, two 3-D ionospheric models were created using the IRI-2016 model (Bilitza et al., 2017), augmented with coincident ionosonde measurements. The combination was performed to create a more realistic ionospheric scenario to test the tomographic algorithms than the one provided by the IRI-2016 model. The electron density distribution gathered from the EISCAT scan was extended to a larger grid from 30° to 80° N latitude, from 15° W to 45° E longitude and up to 800 km altitude. This was done in 4 steps:

1. First, a 3-D background electron density distribution was created for the area-of-interest using the IRI model.
2. Secondly, the vertical electron density profile of this background model was corrected using normalised ionosonde electron density values. Only the vertical profile shape was corrected, because the electron peak density observed from the ISR is generally more accurate. This was performed by normalising the electron density profile from the ionosonde, and multiplying it with the densities in the background IRI model.
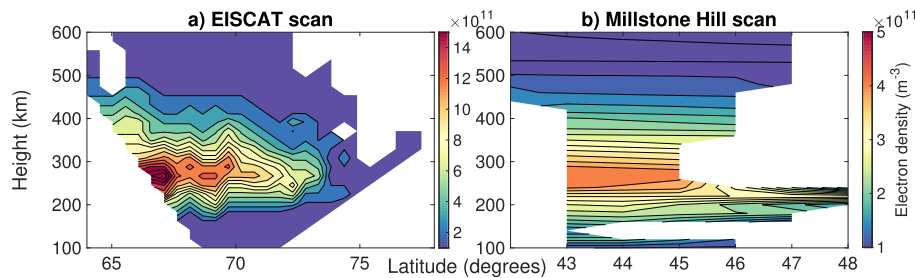
Fig. 2. (a) Original EISCAT radar scan from 2002-01-07at 12:30 UT and (b) Original Millstone Hill ISR scan from 2010-07-30at 16:15 UT.

3. After that, only the values of the background model at the edges of the area of interest were retained, and the electron density values of the ISR scan were added at their respective coordinates and heights.
4. Finally, the gaps between each pixel from the original scan and the boundaries in the new grid were filled by linear interpolation.

In the same way as the first model, observations from the Millstone Hill ISR scan were used to create the second ionospheric model. This model covers latitudes from 20° to 70° N, longitudes from 125° to 70° W and up to 800 km altitude. Fig. 3 shows two latitudinal slices, one for the EISCAT-based model (22° E longitude) and one for the Millstone Hill-based model (72° W longitude).

The ISR scans provide different ionospheric conditions for each of the models. In this case, Millstone Hills ISR data shows a very quiet and stable ionosphere, while EISCAT ISR scan shows more spatial variability. Therefore, the electron density from the EISCAT model will be more challenging to reconstruct using ionospheric tomography.

2.2. Creation of simulated observations associated with the 'truth' ionosphere

These two ionospheric models were used to test three of the most critical issues when imaging the ionosphere with GPS: the impact of satellite and receiver inter-frequency biases, poor receiver coverage of the geographical area-of-interest, and the lack of horizontal rays. If the algorithm is not robust against inter-frequency biases, the vertical TEC may be shifted by a constant value proportional to the biases. The uneven coverage and lack of horizontal raysmay harm the horizontal and vertical accuracy of the reconstructed ionosphere.

For these tests, GPS TEC measurements were simulated to provide input data for the MIDAS ionospheric tomography algorithm. The electron density (see Eq. (1)) was integrated along satellite-to-receiver ray paths through the ionospheric models for a set of actual satellite positions and receiver locations.

To test the effect of the density and distribution of the GPS ground receivers, the receivers of the International GNSS Service (IGS) network in three different geographical areas were chosen: Europe, North Asia and North America. Their geographical distribution can be seen in Fig. 4. The cyan dots represent the GPS receiver positions on each map. The impact of the receiver density in each of these 3 different regions will be compared using the two ionospheric models in Section 2.1. For each comparison all three receiver distributions will be tested using the same ionospheric model which is projected above the region-of-interest. This will provide information about the influence of the receiver distribution and density on the reconstructions.

As shown by Dear and Mitchell (2006), MIDAS can calibrate the TEC without prior knowledge of satellite or receiver inter-frequency biases because it uses the ray-differencing technique described by Andreeva et al. (1992). For this experiment, real satellite biases and realistic receiver biases were added to each TEC measurement to make the simulated observations realistic and to analyse the effect, if any, that the satellite and receiver biases have on the reconstructions.
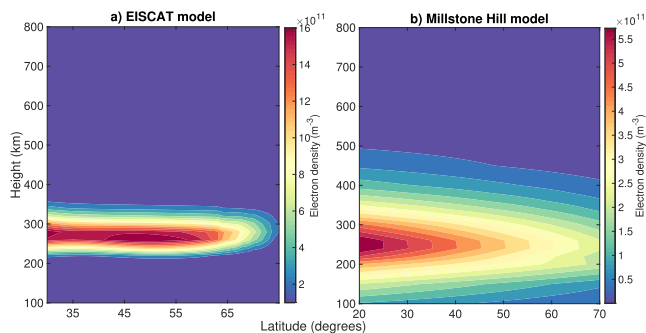

Fig. 3. (a) EISCAT ionospheric model's latitudinal slice at 19° E longitude derived from measurements obtained on 2002-01-07 at 12:30 UT, and (b) Millstone Hill input model's latitudinal slice at 72° W longitude derived from measurements obtained on 2010-07-30 at 16:15 UT.
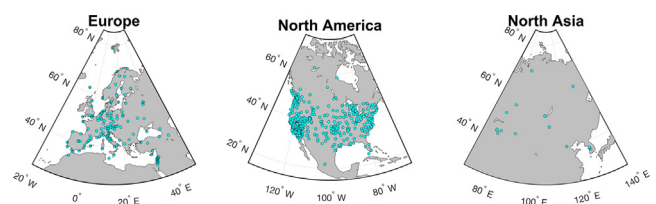

Fig. 4. Location of the GPS receivers used for the reconstruction.

3. Selection of optimal parameters for MIDAS

Once the simulated observations to test the tomographic algorithm are ready, some critical parameters need to be defined to optimise the performance of MIDAS.

3.1. Selection of the optimum reconstruction grid size

The first step after creating the ionospheric models and choosing the receiver networks was to decide the 3-dimensional grid resolution to be used for each experiment. Therefore, a receiver density analysis was done to evaluate the ionospheric reconstructions using different grid resolutions and different numbers of receivers.

For this experiment, receivers were evenly distributed on the grid, and TEC measurements were simulated using the European truth ionosphere as described in Section 2.2. These measurements were inverted with MIDAS into 3-D ionospheric maps, and mean errors in vertical TEC (vTEC) were computed.

In order to provide a comparison between the results of this experiment and a realistic ground receiver distribution, the receiver density of the grids from Fig. 4 was also

analysed. The grids were divided into 5 × 5 degree latitude and longitude bins, and the number of receivers per bin was calculated. This analysis provides a close approximation to the needed grid resolution depending on the receiver density and distribution of each scenario. Fig. 5 shows three examples of receivers evenly distributed over the grid, with red lines to identify the 5 × 5 degree bins.

The simulation was run using 5, 2, 1 and 0.5 degree steps in latitude and longitude and from 4 to 625 receivers equally distributed over the area. Fig. 6 presents the results from the experiment. In Fig. 6b, the mean errors in vTEC as a function of number of receivers per bin are presented. For comparison, In Fig. 6a, the mean (diamond) and standard deviation (line) of the number of receivers per bin are shown for each of the three regions from Fig. 4. As expected, the higher the resolution the smaller the errors obtained, but more receivers are needed to achieve high accuracy results. It's worth mentioning that the distribution of the receivers is optimal in each of the 4 simulated cases. In a real situation, the receivers will not be as evenly distributed and the results will not be as good as in this idealised experiment.

There is a big improvement when moving from a 5° to a 2° grid, but the improvement decreases when moving to smallerpixel sizes. The difference between using 1° and 0.5° steps is very small, around 0.2 TECu when enough receivers cover the area; but the higher the resolution, the longer the computational time. The errors increase dramatically at 1° and 0.5° grids with few receivers per bin due to the insufficient data available to properly reconstruct the ionosphere at such high resolutions. Considering the results obtained in Fig. 6, a resolution of 1° for latitude and longitude was selected for North American and European grids, whereas a step of 2° was used in North Asia.
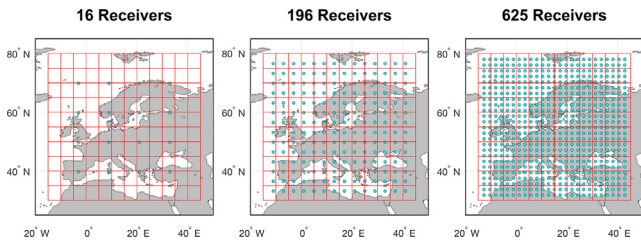

Fig. 5. Three examples of the receivers distribution over the grid and 5 × 5 degree bins.
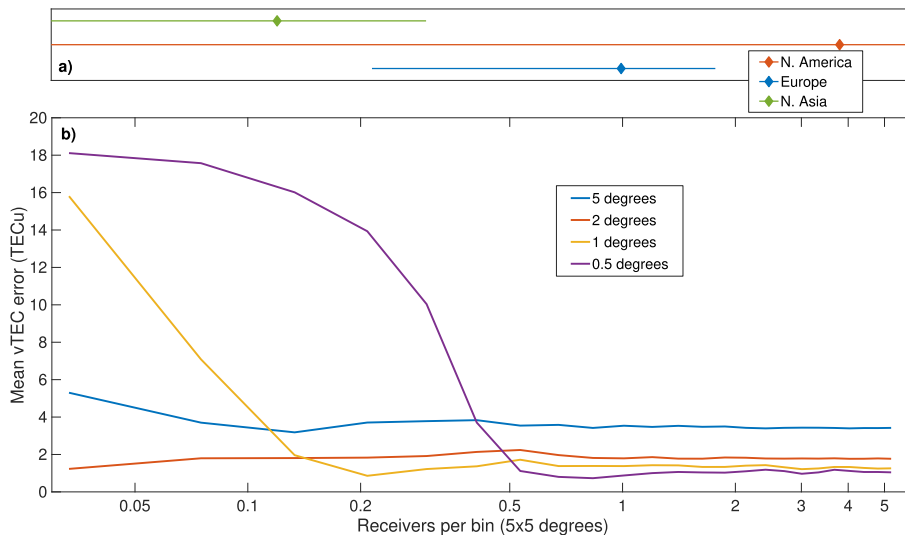

Fig. 6. (a): mean and standard deviation of receivers per bin for the three scenarios under study. (b): mean error in vTEC for different numbers of receivers within each 5 × 5 degree bin. The horizontal axis has a logarithmic scale.

3.2. Orthonormal basis functions to approximate the vertical electron density profile

One of the key features of MIDAS is the use of empirical orthonormal basis functions (EOFs) in the vertical domain (Mitchell and Spencer, 2003; Meggs et al., 2005). These functions provide a realistic approximation of the vertical electron density profile to compensate for the lack of vertical accuracy in the reconstruction, The inversion algorithm fits the ionospheric vertical electron density results to the given EOFs. These orthonormal functions can either be obtained from a set of possible ionospheric profiles derived from models, such as Chapman profiles (Chapman, 1931), or from external data sources such as ionosondes.

Depending on the region of the experiment, an ionosonde close to the time of the ISR observation in Chilton (UK) or Boulder (USA) was used to calculate the EOFs. The ionosonde observations only reach up to the F2 peak height, but the topside of the ionosphere had to be modelled too. In this paper, a novel approach to calibrate the ionosonde is introduced, which uses accurate vTEC values. By keeping the bottomside profiles, the scale heights, H_T, needed to reconstruct the topsides were calculated (using $\alpha - Chapman$ equations (Chapman, 1931)). They were selected to match the ionosonde full profile vTEC with the vTEC obtained from MIDAS at that same location. Using these new topside scale heights, and peak heights and bottomside scale heights derived from the ionosonde data, new Chapman functions were created. This novel method is later referred to as topside calibrated ionosonde.

The inter-frequency bias estimation, horizontal and vertical accuracy of the tomographic algorithm were evaluated in the three regions given in Fig. 4 using two ionospheric models. In Section 4 the obtained results are discussed.

4. Results

In this section, the six reconstructed three-dimensional ionospheric maps are analysed. For clarity, the results concerning each critical feature mentioned in Section 2.2 - bias estimation, horizontal accuracy and vertical electron density distribution - will be investigated separately.

4.1. Bias estimation

First, the impact of the satellite and receiver inter-frequency biases on the results is analysed. MIDAS can calibrate for the biases during the inversion process by using the ray-differencing technique (Andreeva et al., 1992). This feature allows the calculation of the biases by comparing the TEC from the biased input and the TEC from the output of MIDAS for each satellite-to-receiver path. Fig. 7a shows the errors between the calculated and input inter-frequency biases analysing all the satellite-receiver pairs in two areas, the full European grid and in a smaller area in central Europe. The area in central Europe has higher receiver density than the full European region. The relative error, calculated by comparing the estimated absolute value of bias error to the measured TEC of that path, is shown in Fig. 7b. The figure shows how well the biases are estimated for each satellite-receiver pair, with errors smaller than 5% for approximately 99% of the rays in the area with a dense receiver network.

For the next experiment, the TEC values of the simulated observations for each ray-path are multiplied by 10 without modifying the bias values, to test if bias estimation errors depend on the measured TEC. Fig. 8 shows again the absolute and relative errors.

By comparing Figs. 7 and 8 it can be seen that the absolute errors have increased by a factor of 10 in accordance with the increase in TEC, therefore without changing the error percentage. Table 1 shows numerical mean and standard deviation values for the results shown in previous figures.

Finally, TEC results from MIDAS reconstructions using biased and unbiased simulations were compared in order to analyse the effect the inversion method has on the bias estimation. Fig. 9 shows that TEC reconstructions in MIDAS from biased and unbiased TEC simulations are the same, showing that the method is robust for bias estimation.
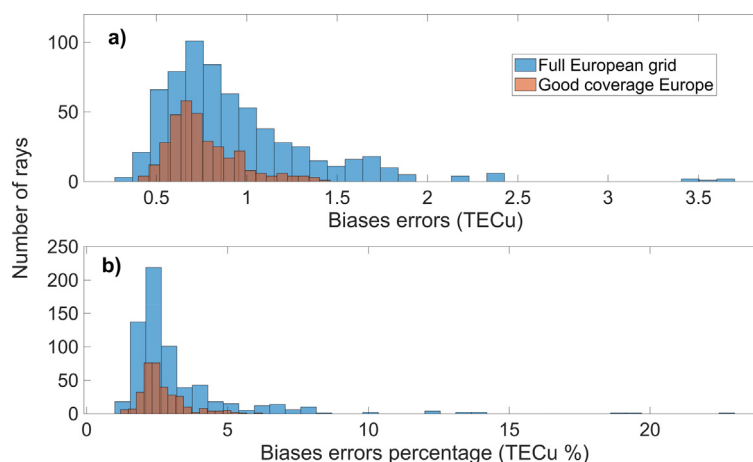

Fig. 7. Histograms of (a) inter-frequency biases estimation errors and (b) inter-frequency biases estimation errors percentage, for each ray over Europe.
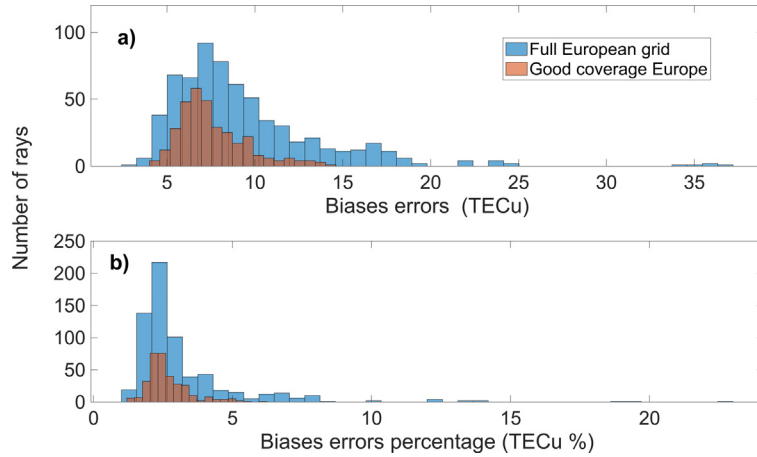
Fig. 8. Histograms of (a) inter-frequency biases estimation errors and (b) inter-frequency biases estimation errors percentage, for each ray over Europe after multiplying the TEC values of the simulated observations by 10.

Table 1
Mean and STD of errors in inter-frequency bias estimation.

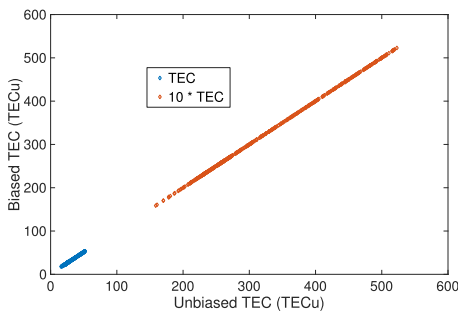|	Full European grid				Good coverage Europe			
	Absolute error		Relative error		Absolute error		Relative error	
	TEC	10 * TEC	TEC	10 * TEC	TEC	10 * TEC	TEC	10 * TEC
Mean (TECu)	0.938	9.388	3.176%	3.175%	0.7564	7.564	2.665%	2.665%
STD (TECu)	0.443	4.429	2.148%	2.147%	0.194	1.942	0.751%	0.751%

Fig. 9. Comparison of reconstructed TEC from simulated TEC data with and without inter-frequency biases.

4.2. Horizontal accuracy

In this section, a detailed analysis of the effect of receiver coverage on the horizontal accuracy of the ionospheric reconstructions is shown, by comparing reconstructed vTEC results with the 'truth' ionospheric models.

The first analysis illustrates the distribution of absolute vTEC errors over the grid, by calculating the vTEC errors relative to the 'truth' ionospheric model. Fig. 10 shows the vTEC errors, limited to 5 TECu. Black dots represent the GPS receiver locations. Results from both ionospheric models show the effect of receiver coverage on the quality of the reconstructed data. The areas with few or no receivers show larger differences from the ionospheric model, which means that the algorithm was not able to reconstruct

the electron density correctly there. Over the mainland, where many receivers are available, the errors are in the range of 0-1 TECu.

Fig. 11 shows relative vTEC errors for the same reconstructions. The colourmap is limited to 10% to highlight the small variations at low percentages. The effect of each model can be derived from this figure. Even if the absolute errors from both models are very similar, results from the EISCAT model, which has higher electron density values, show lower relative errors compared to the Millstone Hill model. It's also worth mentioning that in high receiver density areas the accuracy is 60% to 95% better than in areas with a lower receiver density. When comparing the results from Europe and North America with Asia, the effect of the chosen grid resolution can be seen. The results over Asia show accurate results (1-3 TECu) due to the low resolution of the reconstruction. In order to obtain higher accuracy results (relative errors below 2%), a larger receiver network and a higher resolution reconstruction is needed as seen in the high receiver density areas in Europe and North America.

Overall, with a good coverage of receivers in the area of study, an accurate representation of the ionospheric total electron content can be obtained.

4.3. Vertical accuracy

The accuracy of the vertical electron density distribution of the tomographic image is also an important factor for
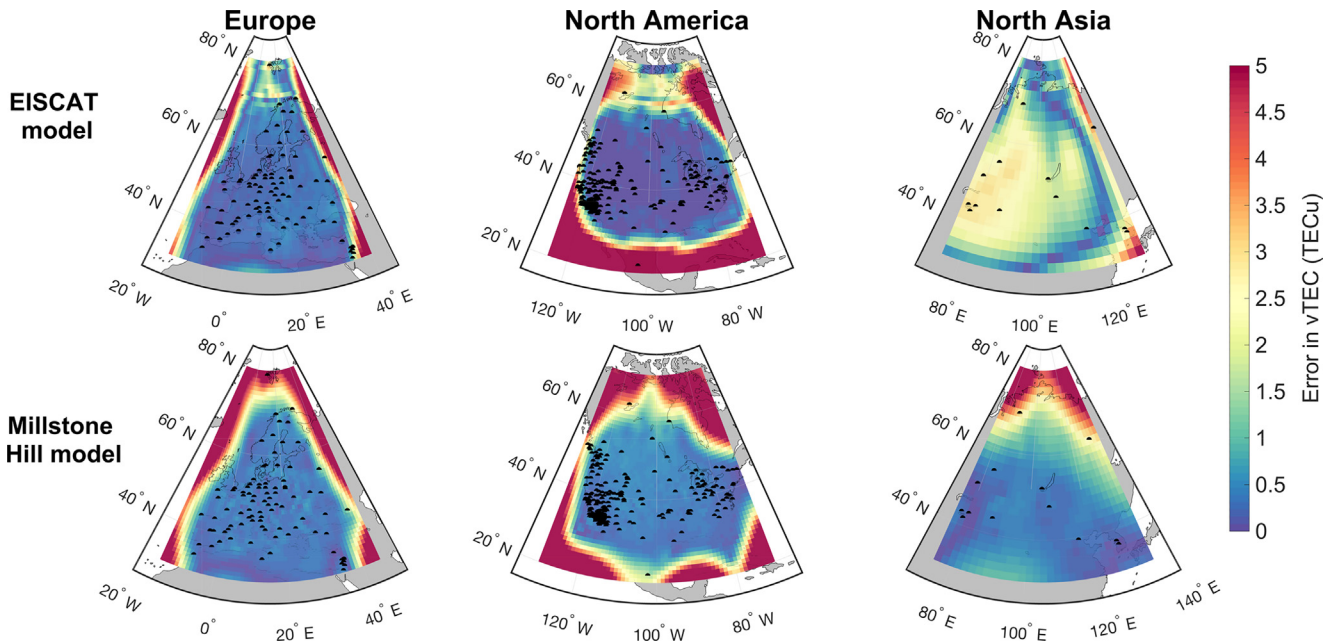
Fig. 10. Maps of the absolute vTEC errors over Europe, North America and North Asia using EISCAT and Millstone Hill input models.
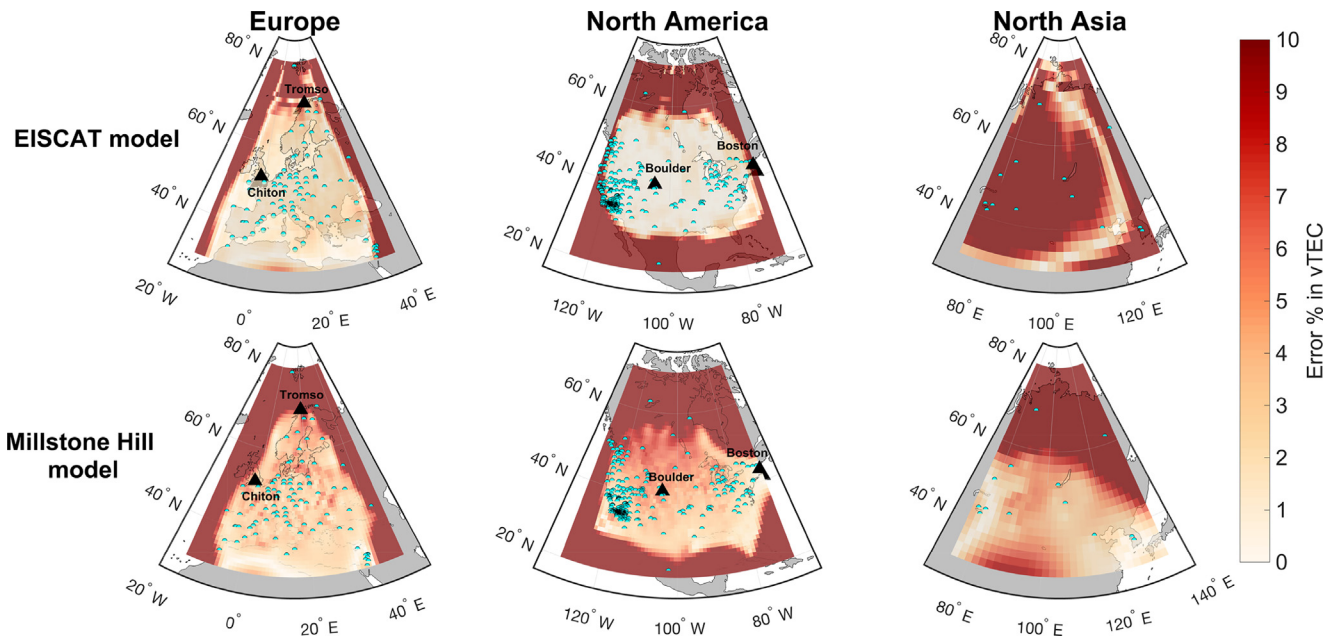

Fig. 11. Maps of relative vTEC error over Europe, North America and North Asia using EISCAT and Millstone Hill input models. The triangles in the maps correspond to the locations of the ionosondes used to create the 'truth' model (Tromsø and Boston) and the ones used to create the vertical EOFs for MIDAS (Chilton and Boulder).

high-precision applications. Therefore, the third goal was to test the vertical accuracy of the MIDAS algorithm. This was done by comparing the vertical electron density distribution of the reconstructions with those of the ionospheric 'truth' models that provide the input of the algorithm. To analyse the influence of the EOFs, ionospheric reconstructions in two regions were investigated: Europe with the EISCAT model and North America with the Millstone Hill model.

Fig. 12 presents the reconstructed vertical electron density profiles for the European region with the EISCAT ionosphere model at Tromsø (scan location) and Chilton (ionosonde location) in the upper row, and for the North-American region with the Millstone hill ionosphere model at Boston (scan location) and Boulder (ionosonde location) in the lower row. These locations are shown in the maps in Fig. 11. The 'true' vertical electron density profile is added for comparison.
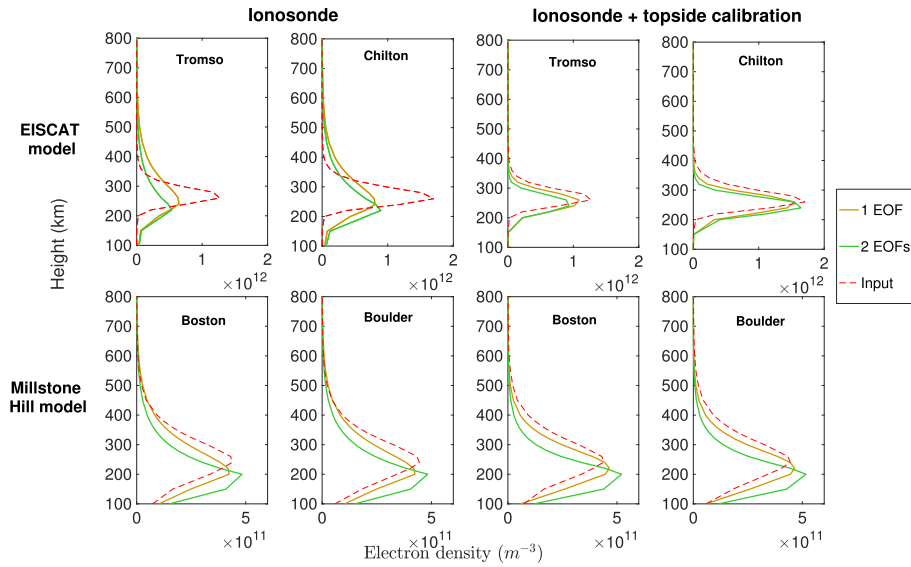
Fig. 12. Reconstructed vertical electron density profiles at Europe (EISCAT model) and North America (Millstone Hill model) obtained using 1 or 2 EOFs, compared with the true vertical electron density distributions at different locations.

Fig. 12 shows that the reconstructed ionospheric peak densities are seriously underestimated when using the EISCAT input model and EOFs derived from ionosonde data. The results using EOFs derived from the topside calibrated ionosonde approach (Section 3.2) show closer agreement to the input profile for the majority of the results. Regarding the scale height, an improvement in the thickness of the F region can also be seen when using EOFs derived from the calibrated ionosonde data.

In Table 2, main parameters of the reconstructed ionosphere and their errors at Tromsø, Chilton, Boston and Boulder are summarised. For both ionospheric models, it can be seen that the results when using only 1 EOF derived from calibrated ionosonde data (the highlighted column in the table) provide a better estimation of the F2 peak electron density. This was the major issue in previous reconstructions.

Analysing the reconstruction of the EISCAT ionospheric model, it can be seen that using EOFs derived from calibrated ionosonde data, the errors in the estimations of the peak electron densities have been reduced by 20–40%. The results of the Millstone Hill ionospheric model, on the other hand, show no major improvement. It can be concluded that the new method to calculate EOFs improves the overall vertical accuracy of this ionospheric electron density imaging algorithm, even at locations far from the ionosonde measuring location. This improvement is only achieved if the original ionosonde profile is significantly different from the input model, which in this experiment only occurs when using the EISCAT model.

5. Conclusions

This study has introduced a novel simulation framework in which a realistic 'truth' ionosphere is created based on ISR measurement data. Using this method,

the accuracy of imaging the ionosphere with MIDAS was evaluated. It was found that the accuracy of the ionospheric reconstruction is influenced by the number of EOFs, their vertical profile and the density of ground based receivers.

This paper demonstrates the importance of the number of GNSS receivers and their distribution over the geographic area under study when imaging the ionosphere. The paper shows errors in vTEC larger than 10% in the ionospheric reconstructions over North Asia. This is caused by the limited resolution due to the small number of receivers distributed over the area. On the other hand, in the regions with sufficient receiver coverage, the errors in vTEC are below 2% for most of the experiments. Another important result is the robustness of MIDAS against both satellite and receiver biases.

This investigation also underlines the importance of the data sets and methods used to derive the EOFs. Even if the obtained vTEC results are very accurate, the vertical electron density distribution differed from the input models in some experiments, with errors over 50% in the peak height and density estimation. Therefore, further experiments were done to improve the vertical shape of the reconstruction. By using the vTEC calibrated ionosonde method, the accuracy of the vertical electron density profile was improved, while the vTEC results remained as accurate as in previous experiments. With only 1 EOF the peak electron density estimation improved by $\sim$ 20–40% in most of the experiments. This method has shown a major improvement in this critical aspect of ionospheric tomography using GNSS data.

The errors when using 2 EOFs are larger in comparison with the errors obtained when using 1 EOF only. This may be caused by the increase in the number of unknowns when increasing the number of EOFs, which makes the problem more difficult to solve when the data are insufficient.

Table 2
Parameters of the reconstructed ionosphere and their errors at **(a)** Tromsø and **(b)** Chilton using the EISCAT ionospheric model; and **(c)** Boston and **(d)** Boulder using the Millstone Hill ionospheric model.

	EOFs from ionosonde data				EOFs from calibrated ionosonde data				Input
a) Tromsø	1 EOF	Error (%)	2 EOFs	Error (%)	1 EOF	Error (%)	2 EOFs	Error (%)	
Peak height (km)	240	20 (7.69%)	220	40 (15.38%)	260	0 (0.0%)	240	20 (7.69%)	260
Peak density ($\times 10^{11} m^{-3}$)	6.47	6.20 (48.95%)	6.04	6.64 (52.36%)	10.85	1.82 (14.42%)	9.62	3.05 (24.01%)	12.68
vTEC (TECu)	11.07	1.66 (17.69%)	7.31	2.09 (22.27%)	9.24	0.16 (1.73%)	7.24	2.16 (22.99%)	9.41
b) Chilton	1 EOF	Error (%)	2 EOFs	Error (%)	1 EOF	Error (%)	2 EOFs	Error (%)	
Peak height (km)	240	20 (7.692%)	220	40 (15.384%)	260	0 (0.0%)	250	10 (4.846%)	260
Peak density ($\times 10^{11} m^{-3}$)	7.78	8.59 (52.47%)	8.03	8.34 (50.94%)	14.66	1.71 (10.47%)	15.14	1.23 (7.53%)	16.37
vTEC (TECu)	13.31	0.23 (1.78%)	12.06	1.01 (7.74%)	12.49	0.58 (4.49%)	11.90	1.17 (8.99%)	13.08
c) Boston	1 EOF	Error (%)	2 EOFs	Error (%)	1 EOF	Error (%)	2 EOFs	Error (%)	
Peak height (km)	200	40 (16.66%)	200	40 (16.66%)	220	20 (8.33%)	200	40 (16.66%)	240
Peak density ($\times 10^{11} m^{-3}$)	4.23	0.13 (3.16%)	4.82	0.45 (10.31%)	4.65	0.27 (6.36%)	5.21	0.83 (19.06%)	4.37
vTEC (TECu)	8.28	0.10 (1.23%)	7.80	0.58 (7.01%)	8.18	0.20 (2.44%)	7.70	0.67 (8.09%)	8.38
d) Boulder	1 EOF	Error (%)	2 EOFs	Error (%)	1 EOF	Error (%)	2 EOFs	Error (%)	
Peak height (km)	200	40 (16.66%)	200	40 (16.66%)	220	20 (8.33%)	200	40 (16.66%)	240
Peak density ($\times 10^{11} m^{-3}$)	4.24	0.19 (4.48%)	4.82	0.38 (8.65%)	4.64	0.20 (4.57%)	5.16	0.72 (16.25%)	4.44
vTEC (TECu)	8.29	0.22 (2.68%)	7.84	0.67 (7.92%)	8.16	0.35 (4.19%)	7.73	0.78 (9.19%)	8.52

The study indicates the importance of data coverage in ionospheric tomography. Additional features in MIDAS incorporating physics-based models (e.g. Da Dalt, 2015) can assists in spatial extrapolation and forecasting. The advantages of these will be evaluated in future work.

Declaration of Competing Interest

The authors declare that they have no known competing financial interests or personal relationships that could have appeared to influence the work reported in this paper.

Acknowledgements

References

Allain, D.J., Mitchell, C.N., 2008. Ionospheric delay corrections for single-frequency GPS receivers over Europe using tomographic mapping. GPS Solut. 13, 141–151. https://doi.org/10.1007/s10291-008-0107-y.

Allain, D.J., Mitchell, C.N., 2010. Comparison of 4D tomographic mapping versus thin-shell approximation for ionospheric delay corrections for single-frequency GPS receivers over North America. GPS Solut. 14, 279–291. https://doi.org/10.1007/s10291-009-0153-0.

Andreeva, E., Kunitsyn, V., Tereshchenko, E., 1992. Phase difference radio tomography of the ionosphere. Geomagnet. Aeronomy/Geomagnetizm i Aeronomiia 32, 104–110.

Austen, J.R., Franke, S.J., Liu, C.H., Yeh, K.C., 1986. Application of computerized tomography tehcniques to ionospheric research. In: Tauriainen, A.. (Ed.), International Beacon Satellite Symposium on Radio Beacon Contribution to the Study of Ionization and Dynamics of the Ionosphere and to Corrections to Geodesy and Technical Workshop, pp. 25–35.

Beynon, W.J.G., Williams, P.J.S., 1978. Incoherent scatter of radio waves from the ionosphere. Rep. Prog. Phys. 41, 909–955. https://doi.org/10.1088/0034-4885/41/6/003.

Bilitza, D., Altadill, D., Truhlik, V., Shubin, V., Galkin, I., Reinisch, B., Huang, X., 2017. International Reference Ionosphere 2016: From ionospheric climate to real-time weather predictions. Space Weather. https://doi.org/10.1002/2016SW001593.

Bust, G.S., Crowley, G., Garner, T.W., Gaussiran, T.L., Meggs, R.W., Mitchell, C.N., Spencer, P.S., Yin, P., Zapfe, B., 2007. Four-dimensional GPS imaging of space weather storms. Space Weather 5, 1–15. https://doi.org/10.1029/2006SW000237.

Bust, G.S., Mitchell, C.N., 2008. History, current state, and future directions of ionospheric imaging. https://doi.org/10.1029/2006RG000212.

Chapman, S., 1931. The absorption and dissociative or ionizing effect of monochromatic radiation in an atmosphere on a rotating earth. Proc. Phys. Soc. 43, 26–45. https://doi.org/10.1088/0959-5309/43/1/305.

Da Dalt, F., 2015. Ionospheric modelling and data assimilation. Ph.D. thesis.

Dear, R.M., Mitchell, C.N., 2006. GPS interfrequency biases and total electron content errors in ionospheric imaging over Europe. Radio Sci. 41. https://doi.org/10.1029/2005RS003269.

Fremouw, E.J., Secan, J.A., Howe, B.M., 1992. Application of stochastic inverse theory to ionospheric tomography. Radio Sci. 27, 721–732. https://doi.org/10.1029/92RS00515.

Gordon, W.E., 1958. Incoherent scattering of radio waves by free electrons with applications to space exploration by Radar. Proc. IRE 46, 1824–1829. https://doi.org/10.1109/JRPROC.1958.286852.

Hargreaves, J.K., 1992. The Solar-Terrestrial Environment. https://doi.org/10.1017/CBO9780511628924.

Hernández-Pajares, M., Juan, J.M., Sanz, J., 1999. New approaches in global ionospheric determination using ground GPS data. J. Atmos. Solar Terr. Phys. 61, 1237–1247. https://doi.org/10.1016/S1364-6826(99)00054-1.

Hernández-Pajares, M., Juan, J.M., Sanz, J., Colombo, O.L., 2000. Application of ionospheric tomography to real-time GPS carrier-phase ambiguities resolution, at scales of 400–1000 km and with high geomagnetic activity. Geophys. Res. Lett., 27

Hernandez-Pajares, M., Juan, J.M., Sanz, J., Solé, J.G., 1998. Global observation of the ionospheric electronic response to solar events using ground and LEO GPS data. J. Geophys. Res. 103, 20789–20796. https://doi.org/10.1029/98JA01272.

Lee, J.K., Kamalabadi, F., Makela, J.J., 2008. Three-dimensional tomography of ionospheric variability using a dense GPS receiver array. Radio Sci. 43, 1–15. https://doi.org/10.1029/2007RS003716.

Leitinger, R., 1999. Ionospheric tomography. In: The Review of Radio Science 1996-1999 Chapter 24, IEEE, pp. 581–623, https://doi.org/10.1109/9780470546352.ch1.

Mannucci, A.J., Wilson, B.D., Yuan, D.N., Ho, C.H., Lindqwister, U.J., Runge, T.F., 1998. A global mapping technique for GPS-derived ionospheric total electron content measurements. Radio Sci. 33, 565–582. https://doi.org/10.1029/97RS02707.

McNamara, L.F., 1991. The Ionosphere: Communications, Surveillance, and Direction Finding. Orbit, A Foundation Series. Krieger Publishing Company.

Meggs, R.W., Mitchell, C.N., Howells, V.S.C., 2005. Simultaneous observations of the main trough using GPS imaging and the EISCAT radar. Ann. Geophys. 23, 753–757. https://doi.org/10.5194/angeo-23-753-2005.

Mitchell, C.N., Jones, D.G., Kersley, L., Pryse, S.E., Walker, I.K., 1995. Imaging of field-aligned structures in the auroral ionosphere. Annales Geophys. 13, 1311–1319.

Mitchell, C.N., Spencer, P.S., 2003. A three-dimensional time-dependent algorithm for ionospheric imaging using GPS. Ann. Geophys. 46, 687–696. https://doi.org/10.4401/ag-4373.

Pryse, S.E., Kersley, L., 1992. A preliminary experimental test of ionospheric tomography. J. Atmos. Terr. Phys. 54, 1007–1012. https://doi.org/10.1016/0021-9169(92)90067-U.

Radon, J., 1917. Uber die Bestimmung von Funktionen durch ihre Integralwerte langs geweisser Mannigfaltigkeiten (on the determination of functions from their integrals along certain manifolds). Berichte Saechsische Akademie der Wissenschaften 29, 262–277.

Rishbeth, H., Williams, P.J.S., 1985. The EISCAT Ionospheric Radar - the System and its early results. Roy. Astronom. Soc. Quart. J. 26, 478–512.

Rose, J.A., Watson, R.J., Allain, D.J., Mitchell, C.N., 2014. Ionospheric corrections for GPS time transfer. Radio Sci. 49, 196–206. https://doi.org/10.1002/2013RS005212.

Walker, I.K., Heaton, J.A., Kersley, L., Mitchell, C.N., Pryse, S.E., Williams, M.J., 1996. EISCAT verification in the development of ionospheric tomography. Ann. Geophys. https://doi.org/10.1007/s00585-996-1413-8.

Wilson, B.D., Mannucci, A.J., 1993. Instrumental biases in ionospheric measurements derived from GPS Data, In: Proceedings of the 6th International Technical Meeting of the Satellite Division of The Institute of Navigation (ION GPS 1993), pp. 1343–1351.